Petroleum Science 19 (2022) 2683–2694

Contents lists available at ScienceDirect

Petroleum Science

journal homepage: www.keaipublishing.com/en/journals/petroleum-science

Original Paper

Effect of microscopic pore structures on ultrasonic velocity in tight sandstone with different fluid saturation

Jian-Yong Xie [a], Jun-Jie Zhang [a, *], Wei Xiang [b], Yan-Ping Fang [a], Ya-Juan Xue [c], Jun-Xing Cao [a], Ren-Fei Tian [a, d]

[a] State Key Laboratory of Oil and Gas Reservoir Geology and Exploitation, Chengdu University of Technology (CDUT), Geophysical Institute, Chengdu, Sichuan, 610059, China
[b] Oilfield Technology Division, China National Offshore Oilfield Services Co., Zhanjiang, Guangdong, 524000, China
[c] School of Communication Engineering, Chengdu University of Information Technology, Chengdu, Sichuan, 610225, China
[d] State Key Laboratory of Natural Gas Hydrate, Beijing, 100028, China

ARTICLE INFO

Article history:
Received 19 November 2021
Received in revised form
17 January 2022
Accepted 14 June 2022
Available online 16 June 2022

Edited by Jie Hao

Keywords:
Tight sandstone
Pore structure
Casting thin section
Ultrasonic measurement

ABSTRACT

Microcosmic details of pore structure are the essential factors affecting the elastic properties of tight sandstone reservoirs, while the relationships in between are still incompletely clear due to the fact that quantitative or semi-quantitative experiments are hard to achieve. Here, three sets of tight sandstone samples from the Junggar Basin are selected elaborately based on casting thin sections, XRD detection, and petro-physical measurement, and each set is characterized by a single varied microcosmic factor (pore connectedness, pore type, and grain size) of the pore structure. An ultrasonic pulse transmission technique is conducted to study the response of elastic properties to the varied microcosmic details of pore structure in the situation of different pore fluid (gas, brine, and oil) saturation and confining pressure. Observations show samples with less connectedness, inter-granular dominant pores, and smaller grain size showed greater velocities in normal conditions. V_p is more sensitive to the variations of pore type, while V_s is more sensitive to the variations of grain size. Samples with better connectedness at fluid saturation (oil or brine) show greater sensitivity to the confining pressure than those with gas saturation with a growth rate of 6.9%–11.9%, and the sensitivity is more likely controlled by connectedness. The pore types (inter-granular or intra-granular) can be distinguished by the sensitivity of velocities to the variation of pore fluid at high confining pressure (> 60 MPa). The samples with small grain sizes tend to be more sensitive to the variations of confining pressure. With this knowledge, we can semi-quantitatively distinguish the complex pore structures with different fluids by the variation of elastic properties, which can help improve the precision of seismic reservoir prediction for tight sandstone reservoirs.

1. Introduction

Elastic properties from seismic exploration are crucial for the interpretation of lithology, pore fluid, and geological structure in the conventional or unconventional reservoirs. Knowledge of the corresponding responses of elastic properties to the variations of each possible affected factor becomes of growing importance in geophysics, petrophysical and geological engineering, especially for increasing the precision of seismic interpretation.

Tight sandstones, as an important unconventional gas reservoir, will play a significant role in the future energy supply (Hughes, 2013; Sakhaee-Pour, 2014). Because of its intricate diagenetic environment and geologic history, the pore structure in tight sandstone is extremely complicated and determined by the interaction of multiple affecting factors such as pore connectedness, pore type, grain size, cementation type, etc. Such characterizations of pore structure in turn lead the petrophysical characterizations and seismic responses of tight sandstone reservoirs to greatly deviate from those of conventional reservoirs (Masters, 1979; Law and Dickinson, 1985; Spencer, 1989; Surdam, 1997; Si et al., 2016). Additionally, the hydrocarbon storage and calculations and sealing

* Corresponding author.
E-mail address: 839910719@qq.com (J.-J. Zhang).

https://doi.org/10.1016/j.petsci.2022.06.009

capacity may also be affected by the pore type, size, and arrangement (Dawson and Almon, 2002; Dewhurst et al., 2002; Ambrose et al., 2012). Recently, several studies have tried to figure out the relationship between the pore structure and other intrinsic properties of tight sandstones, such as elastic properties (Nelson, 2009; Smith et al., 2009; Ruiz and Cheng, 2010; Yan and Han, 2015; Ba, 2017; Cheng, 2019; Zhang, 2021), estimated ultimate recovery (EUR) (Sakhaee-Pour, 2014) and multifractal properties (Ge et al., 2015). For this purpose, multiple experimental techniques were applied, e.g. scanning electron microscopy (SEM), mercury intrusion porosimetry (MIP), digital image analysis (Weger et al., 2009; Verwer et al., 2010, 2011), nuclear magnetic resonance (NMR), and X-ray micro-computed tomography (micro-CT) (Dong and Blunt, 2009; Blunt et al., 2013; Peng et al., 2014; Gao and Li, 2015). However, due to the complexity and random distributions of pore structure in natural rocks or lack of cored samples, they may not take into account the variations of each component of pore structure separately, which makes the topic hard to be solved with experimental measurement. On the other hand, various theoretical models have been established to study the influence of types of the pore (Mousavi and Bryant, 2007; Sakhaee-Pour, 2014), pore network (Ebrahimi et al., 2013; Yang et al., 2013; Ma et al., 2014; Xu et al., 2014) and pore size distribution (Clarkson et al., 2012; Oukhlef et al., 2014) on the physical properties of tight sandstones. However, theoretical models are commonly based on multiple simplified assumptions and restricted to specific lithologies and certain sizes, thus impeding their generalization. As a result, the relationships between the pore structure and seismic attributes, especially in the conditions of different fluid saturation and confining pressure, are still far from being well understood.

An alternative approach to overcome such a challenge is to employ the experimental control varied method. Such a method allows the clear identification of cause and effect because only one factor is different at a time so that the effect of that single factor can be determined. It is an effective toolkit to figure out the separate influence of pore structure on acoustic velocities in different conditions. Many pieces of research try to construct well-controlled artificial rock samples to deal with the quantitative measurements (Xie, 2019; Ding, 2020) and make many differences. However, experimental study on natural samples would be more convincing. In this paper, we implement the controlling variate methods by combining the usage of qualitative geological descriptions with experimental rock physical measurements on elaborately selected natural samples. Firstly, 95 cylindrical sandstone samples from 27 wells in 4 regions in the target exploration strata of the Jurassic age in the middle region of the Junggar Basin in China are collected for petrophysical measurements. Secondly, casting thin sections are examined to semi-quantitatively or qualitatively describe each component (septicity, gradation, grain support type, contact among grains, cementation, pore connectedness, pore type, and grain size) of the pore structure in the aforementioned multiple series of cored tight sandstones. Simultaneously, XRD (X-ray diffraction) is used to detect the percentages of each mineral in the samples. On this basis, three sets of samples are selected, in which each set of samples is characterized by only one varied factor of pore structure (pore connectedness, pore type, and grain size respectively), and every other parameter is similar. Additionally, samples in each selected set are drilled from the same borehole with similar burial depth and density. Thirdly, the ultrasonic pulse transmission method is performed to measure the P-wave and S-wave velocities of samples with different fluid saturations (gas, brine, and oil) under different confining pressures. Comparisons among the responses of velocities are made to try to find the corresponding independent relationship, which can be applied to the qualitative or semi-quantitative prediction of each element of the pore structure. Such responses have the potential for the identification of pore structure from seismic profiles in field reservoir studies.

2. Sample description and petrophysical measurements

Samples in our core repository are drilled from target exploration strata (J1b, J1s and J2x) of Jurassic age from the middle region of the Junggar Basin in China. The basin is the second-largest inland basin in China and is located in the northwest of Xinjiang province. The core repository consists of 95 cylindrical sandstone samples, and all the samples were cut and grounded into 25 mm in diameter by 50 mm in length, which are used for petrophysical tests (Fig. 1). The porosity is measured with a helium porosimeter, which acts in line with the gas (helium) expansion law, following the Boyle Law. Fig. 2 shows the plot of density against porosity for the data set, which exhibits a linear relationship. The porosities of samples are generally less than 15%, and most of them are lower than 10%. An X-ray diffraction technique was conducted to detect the mineral components of the samples. With the casting thin section test, we can statistically determine the granularity, septicity, gradation, pore type, connectedness, distribution, and combination characterization of the samples. The casting thin section is made by pressurized injecting dyeing resin or colored liquid adhesive into the pore space of rock under vacuum conditions, pending the solidification of the injected adhesive, mounting on a glass slide and then ground smooth using progressively finer abrasive (30 μm thickness). After careful comparison and analysis of the basic parameters of cores, three sets of samples are selected, in which each set of samples is characterized by only one varied factor of pore structure (pore connectedness, pore type, and grain size, respectively) and every other parameter being similar (Table 1, Table 2, and Table 3). Samples in each selected set are drilled from the same borehole with a similar buried depth and density. As a result, we can satisfy the requirements of the control variate method and employ this method to study the influence of the corresponding component of the pore structure on the dynamic properties in tight sandstone.

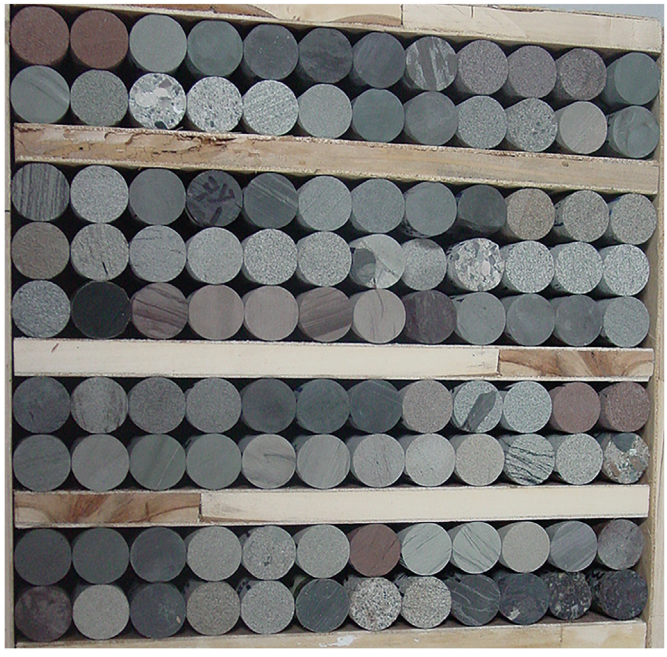

Fig. 1. Picture of the core repository in the laboratory.

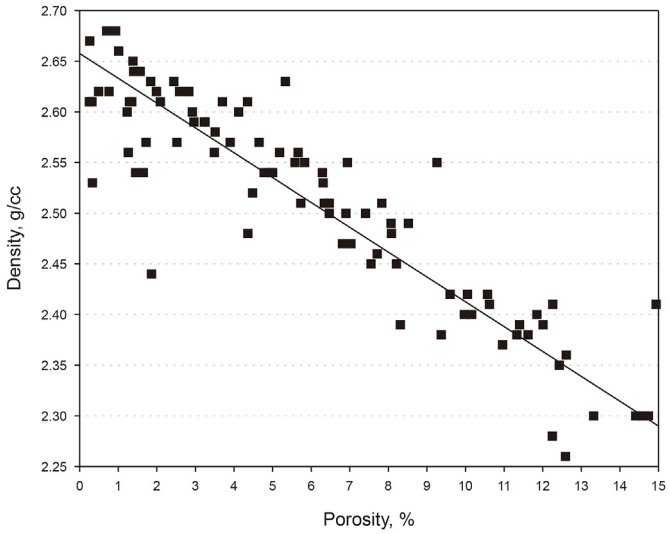

Fig. 2. Crossplot of porosty and density for series of samples.

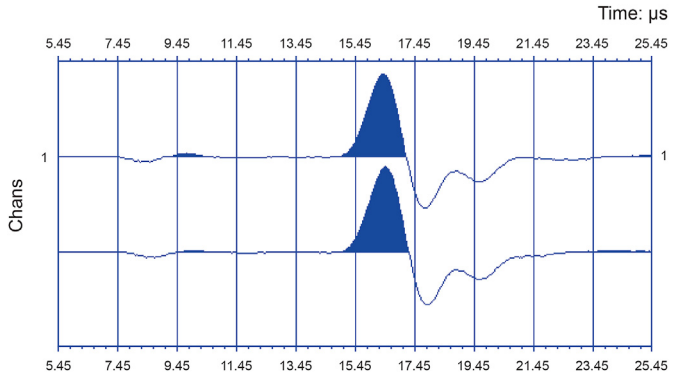

Fig. 3. Observations of shear wave transducers by rotating in two mutual vertical directions.

3. Ultrasonic measurement under different pore fluid and confining pressure

Ultrasonic velocities (V_p & V_s) are measured simultaneously by the pulse transmission technique (Birch, 1960) with ultrasonic transducers at 0.5 MHz central frequencies. It is noted that anisotropy is always a necessary factor that needs to be concerned when dealing with the velocity measurement of a rock sample. It is intuitive to see some lamina in several samples in the core repository as shown in Fig. 1, and it is natural to recognize them as anisotropic samples. Even the samples without evident lamina can be anisotropic due to the distribution of microstructures, or both cases above can be isotropic since the velocity anisotropy is the result of the interacted effect of multiple factors. In this sense, we have tried to detect the shear wave splitting by rotating the shear wave transducers on the three sets of samples. As shown in Fig. 3 for the #Yong samples, the S-wave waveform remained nearly unchanged with the rotation, which means the sample tends to be characterized as isotropic. The bulk density was calculated from saturated and dry weights and measured cylinder volumes. The samples were placed into an oven with a temperature of 60 °C for more than 3 days and exposed to the normal condition with room temperature (23–25 °C) and 50%–60% humidity for about 2 days for equilibration before the measurements of the dry situation. Following the dry measurement, samples were saturated with desired brine by storing them in a vacuum for at least 12 h (Verwer et al., 2010). Brine with 3% NaCl was used here to prevent potential chemical reactions. Oil saturation was achieved by using a suction effect in a vacuum under a pressure of at least 2 bar sustained for at least 10 days. The term “full saturation” here does not mean that the pores in the sample are 100% saturated with oil, but means the sample can't enter any more oil into the sample whatever the pressure and time are. On this basis, ultrasonic velocities were measured on the samples at elevated confining pressures (0, 6, 10, 20, 30, 40, 50, and 60 MPa). The sample was installed with a shrinkable jacket and then the jacketed sample was placed between ultrasonic transducers (P-wave or S-wave) (Fig. 4a). The center frequency of the transducers in the system was 0.5 MHz. The acoustic assembly was finally placed into the pressure vessel of the RETS2000/120 electrohydraulic servo-controlled Rock Elasticity Testing System (SRETS) in CUPB, China (Fig. 4b). All the experiments were measured at room temperature. The waveforms will be obtained 15 min after the confining pressure reaches each pre-set

Table 1
Basic parameters for the # Sha series tight sandstone in normal conditions.

#Sha	Depth, m	Porosity, %	Density, g/cm^3	Quartz	Feldspar	Debris	Mica	Clay	Calcareous
40	4325	8.08	2.48	45%	17%	25%	5%	8%	0%
41	4309.8	8.21	2.38	45%	25%	24%	4%	5%	7%
42	4315.5	9.37	2.38	46%	18%	25%	2%	4%	5%

Table 2
Basic parameters for the #Yong series tight sandstone in normal conditions.

#Yong	Depth, m	Porosity, %	Density, g/cm^3	Quartz	Feldspar	Debris	Mica	Clay	Calcareous
6-6	6085.1	5.18	2.56	40%	20%	24%	4%	4%	6%
7-2	6100.5	5.83	2.55	37%	20%	28%	2%	6%	4%

Table 3
Basic parameters for the #Zheng series tight sandstone in normal conditions.

#Zheng	Depth, m	Porosity, %	Density, g/cm^3	Quartz	Feldspar	Debris	Mica	Clay	Calcareous
11-2	4416.2	13.32	2.3	45%	15%	25%	4%	7%	4%
11-5	4423	12.25	2.28	40%	19%	26%	3%	5%	7%

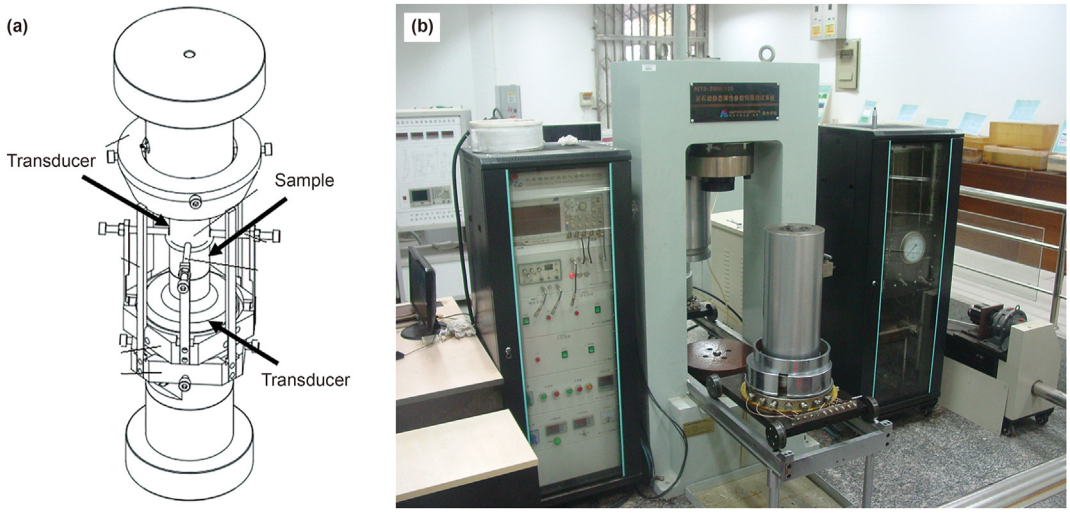

Fig. 4. (a) Schematic diagram of the three-component ultrasonic test facility with a dominant frequency of 0.5 MHz and (b) Picture of the RETS2000/120 electro hydraulic servo-controlled rock elasticity testing system.

value. Based on the method of error analysis for ultrasonic pulse transmission technique from Yin (1992) and Hornby (1998), the errors for P- and S-wave velocities are estimated at approximately 0.8% and 1.2%, respectively.

4. Results and analysis

4.1. Pore connectedness versus velocities

Pore connectedness is pivotal to determining the transport properties of porous rocks. Though high pore connectedness generally results in high permeability, the permeability is also determined by several other parameters. In this section, we tried to figure out the relationship between pore connectedness and velocities in different conditions to seek the possible specific response of velocities to predict the pore connectedness. Fig. 5a shows the picture of the #Sha series of tight sandstone samples. The basic physical properties of the samples in normal conditions are shown in Table 1. XRD analysis showed that samples #Sha 40, # Sha41, and #Sha 42 have similar mineral components and weight percentages, and they are cored in the same borehole from a similar depth. Based on the statistical analysis of multiple cast thin section images (more than 20 images for each sample), specific descriptions of the pore structure are shown in Table 4. Fig. 5b, c, and d showed typical images for the #Sha samples. In terms of microstructure, they showed a similar range of grain size, septicity, gradation, grain support type, contact among grains, cementation type, and pore type, and the only difference among the samples is the connectedness between the pores. The pore connectedness in sample # Sha 40 is poor, the pores of # Sha 41 are medium connected, and # Sha 42 exhibited good connectedness. As shown in Table 4, the corresponding velocities (for both P-wave and S-wave) of poorly connected samples are generally greater than those of relatively well-connected ones ($V_{40} > V_{41} > V_{42}$). It is noted that the velocities listed in the table are measured with ultrasonic transducers in the dried samples under the condition of normal temperature and pressure. To further analyse the effects of pore connectedness on the seismic response of tight sandstone in a different circumstance, we saturated all the samples with gas, brine, and oil, and investigated the response of velocities under different confining pressures. Fig. 5 shows the response of P- and S-wave velocities when confining pressure is increased from 2 MPa to 60 MPa under different fluid saturations (air, brine, and oil) for the samples # 40, # 41, and # 42. As illustrated in Fig. 5a and b, in the case of gas saturation, when the compliant pores have been closed under low confining pressure, both P-wave and S-wave velocities of samples with poor connectedness are always greater than those with good connectedness at the same confining pressure ($V_{40} > V_{41} > V_{42}$). Since the poorly connected samples exhibited relatively low porosity as shown in Table 1, it is reasonable to expect that the velocity would decrease with the increasing porosity and that the better connectedness would lead to lower velocity when every other factor is similar. In the case of gas saturation for the samples with different connectedness, as shown in Fig. 6a and b, both the P-wave and S-wave velocities of the #Sha samples have similar sensitivity to increasing confining pressure in the range of 2 MPa–60 MPa, the growth rates are approximately 17% and 15% for V_p and V_s, and V_p tends to be more sensitive to pressure than V_s. The similarity of the growth of the velocities to the pressure indicates that the samples are characterized by similar amounts of compressible soft pores. Additionally, both P-wave and S-wave velocities of #Sha series samples reach a maximum of approximately 50 MPa, which means the aspect ratios of the compressible soft pores are also similar. In the case of water saturation, as shown in Fig. 6c and d, at low confining pressure (e.g. 2 MPa), the differences among the velocities of the three samples are less than those in a gas situation. It can be reasonably explained that samples with better connectedness exhibited greater porosity and thereby needed more water to be saturated, which can mitigate the differences in velocities aroused by the variation of porosity. With the increasing confining pressure (2–60 MPa), velocities of a sample with worse connectedness showed greater sensitivity to the confining pressure with a V_p growth rate of 8.7%–10.6% for the #Sha samples (Table 5). Similar phenomena can be observed for the shear wave velocities. Further, under the confining pressure and water saturation, samples with better connectivity are more likely to have localized flow of water in the pore space through the pore roar channel under ultrasonic excitation, and the flow of fluid will cause friction with the throat wall during the flow process, thus causing energy dissipation, and the increase in confining pressure will strengthen this effect, resulting in a slowing down of the increasing velocity trend, and further rigorous rock physical modeling is needed to explain the mechanisms. In the case of oil saturation, as shown in Fig. 6e and f, the velocities of the well-connected sample (#Sha 42) are overall

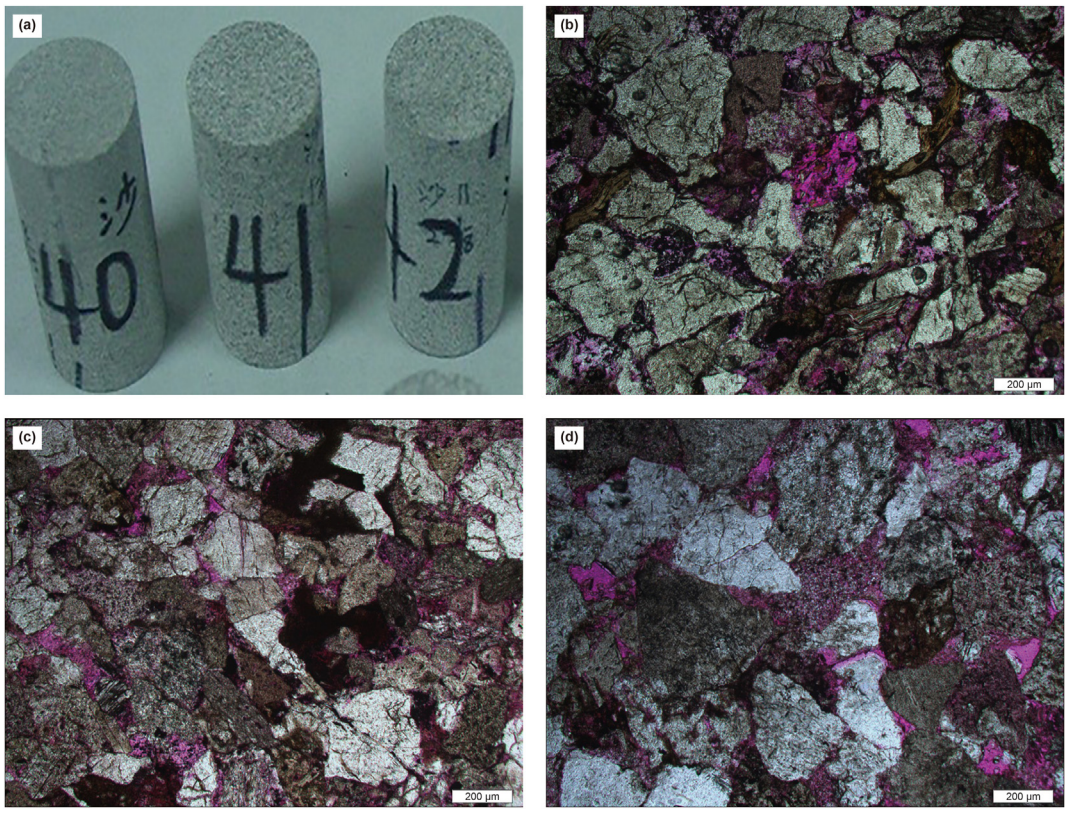

Fig. 5. (a) Picture of the # Sha series of tight sandstone samples, typical casting thin section images of samples (100X, plane-polarized light) (b) #Sha 40, poor connected, (c) #Sha 41, medium connected, (d) #Sha 42, good connected.

Table 4
Characterization of microstructure for # Sha series tight sandstone. (AS–Angularity Subround, M–Medium, GST–Grain-supported type, CAG–Contact among grains, PSLC–Primarily spot-line contact, CT–Cementation type, IDP–Inter-granular dissolved pores).

#Yong	GS, mm	V_p, m/s	V_s, m/s	Psephicity	Gradation	GST	CAG	CT	PT	Connectedness
40	0.25–0.50	3432	2260	AS	M	GS	PSLC	PC	IDP	Poor
41	0.25–0.50	3358	2200	AS	M	GS	PSLC	PC	IDP	Medium
42	0.3–0.50	3013	2007	AS	M	GS	PSLC	PC	IDP	Fair

greater than those of the moderately connected sample (#Sha 41), which may be attributed to the fact that the amount of saturated fluid replaces porosity as the main controlling factor affecting velocity. Both the above-mentioned samples are smaller than those of the poorest connected samples (#Sha 40.). Generally, the sensitivity of velocities to the confining pressure for the sample with fluid saturation (oil and brine) is weak compared to the case of gas saturation, while the mechanisms for the response of velocities to the confining pressure and fluid saturation are more complicated when considering a variation of connectedness than those of gas saturation.

4.2. Pore type on the velocities

Pore types in tight sandstone can be classified into as many as seven types (interparticle, intraparticle, inter crystal, melodic, fenestral, fracture, and vugs). The pore types have a great influence on the producibility of hydrocarbons (Sakhaee-Pour, 2014), reservoir permeability heterogeneity, wettability, and seismic velocity variation (Anselmetti and Eberli, 1999; McCreesh et al., 1991; Passey et al., 2010).

In this section, we focus on discussing the influence of two significant pore types, the inter-granular (pore between particles) and intra-granular (pore within individual particles or grains) mineral pores, on the acoustic properties in tight sandstone under varied fluid saturation at different confining pressures. Compared to the intra-granular pores, the inter-granular pores are more likely to form a permeable pore network since they have a higher probability of being interconnected, while the intra-particle pores are commonly connected to the overall pore system and the associated pore throats may be smaller and relatively fewer (McCreesh et al., 1991). The shapes of inter-granular pores are elongated without strong preferential orientation, while the shape of an intra-granular pore is commonly determined by its origin (Loucks et al., 2012). As shown in Table 2, samples # Yong 6-6 and # Yong 7-2 have similarities in burial depth, porosity, density, type, and percentage of interstitial material and mineral components. Moreover, based on the observations on casting thin section images, as shown typically in Fig. 7a and b, they also showed a similar range of grain size, septicity, gradation, grain support type, contact among grains, cementation type, and connectivity (Table 6). The only difference between the two samples is the pore type. # Yong 6-6 is dominated by the inter-particle dissolution pore, and # Yong 7-2 is mainly comprised of the intra-granular dissolved pore. As shown in

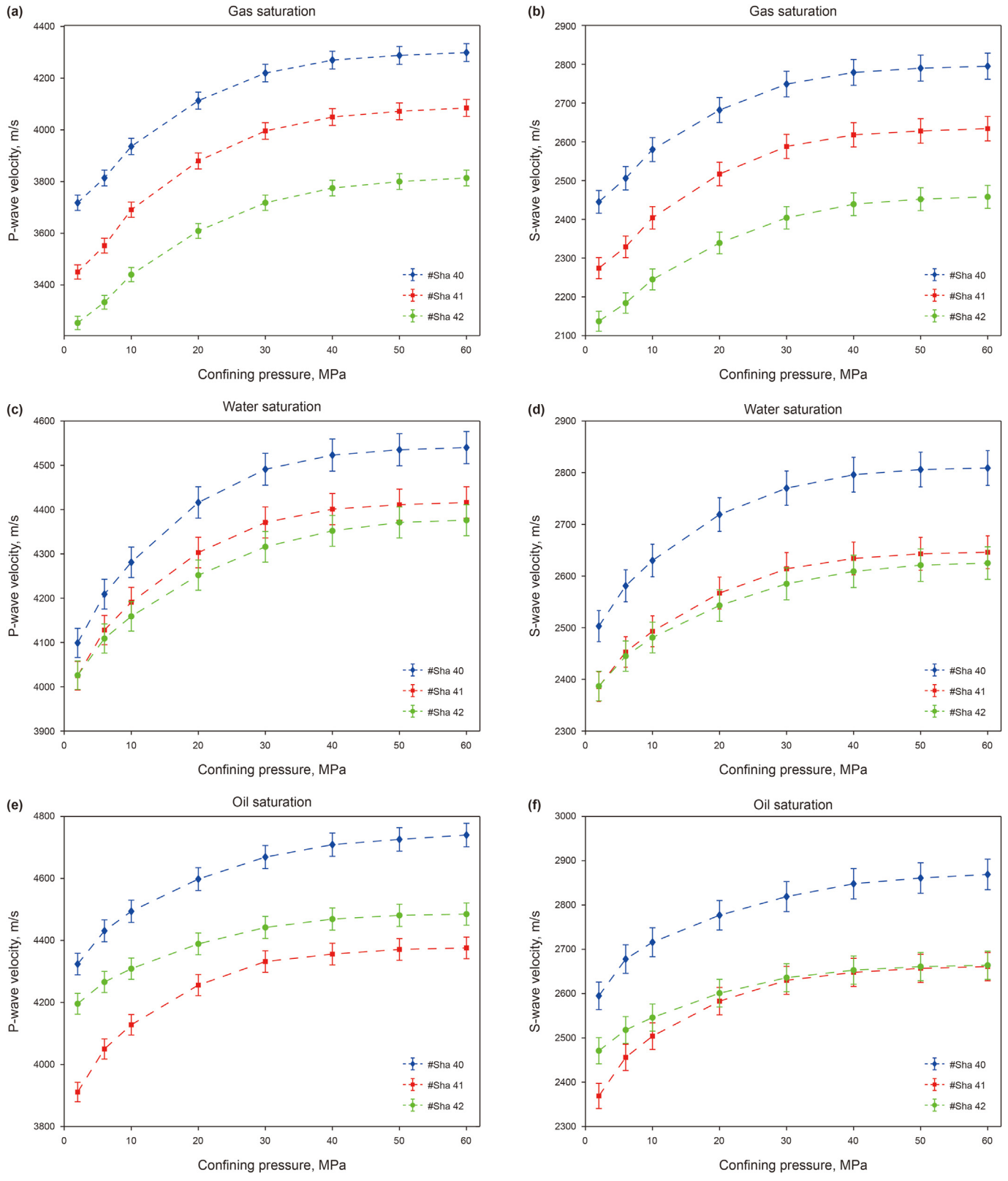

Fig. 6. Response of P- and S-wave velocities when the confining pressure is increasing under different fluids saturation. (a), (b) showed V_p and V_s in the condition of gas saturation; (c), (d) showed V_p and V_s in the condition of brine saturation; (e), (f) showed V_p and V_s in the condition of oil saturation for the samples # Sha 40, 41 and 42.

Table 5
Relative variation ratio of velocities for #Sha samples under different fluid saturation when confining pressure increase from 2 MPa to 60 MPa.

#Sha	Velocity	Gas	Oil	Water
40	V_p	15.6%	6.9%	10.8%
	V_s	14.3%	7.8%	12.2%
41	V_p	18.3%	11.9%	9.75%
	V_s	15.8%	12.3%	10.9%
42	V_p	17.2%	9.6%	8.7%
	V_s	15.0%	10.6%	10%

Table 6, both the P-wave velocity (3617 m/s) and S-wave (2305 m/s) velocity of # Yong 6-6 are higher than those of # Yong 7-2 in normal pressure and temperature, and the pore type is shown to have more influence on P-wave velocity. For further study of the influence of pore type on the properties of tight sandstone. We saturated both samples with gas, brine, and oil to investigate the response of the sample under different confining pressures. Fig. 8 shows the response of P- and S-wave velocities when the confining pressure is increased from 2 MPa to 60 MPa under different fluid saturations. In each case, the P- and S-wave velocities tend to increase with the confining pressure. However, P-wave velocity in the case of gas saturation tends to be more sensitive to the increasing confining pressure than that in the case of water and oil saturation for both samples. It can be reasonably explained by the fact that fluid in the pore will moderate the influence of confining pressure, and further alleviate the variation of velocities. Another interesting phenomenon can be observed that both the P-wave and S-wave velocities of a fluid saturated sample are always greater than the gas-saturated sample regardless of the increasing confining pressure for the sample # Yong 6-6, and velocities in oil saturation are greater than water saturation (Fig. 8a and b). For sample # Yong 7-2 which is mainly comprised of the intra-granular dissolved pores, as shown typically in Fig. 8c and d, the velocities of the above three cases (air, brine, and oil-saturated) tend to get close to each other with the increasing confining pressure. As the confining pressure reaches 60 MPa, the velocities in such three cases are almost identical. Consequently, the difference among the velocities in the fluid saturation at high confining pressure is likely a good indicator to distinguish the pore type. Fig. 9 shows the response of P-wave and S-wave velocities in samples # Yong 6-6 and # Yong 7-2 with increasing confining pressure in the case of air, brine, and oil saturation, respectively. As shown in Fig. 9a and b, in the condition of gas saturation and relatively low confining pressure (<25 MPa), both P-wave and S-wave velocities for the sample # Yong 6-6 are greater than those of the sample # Yong 7-2, when the confining pressure exceeds 25 MPa, opposite results can be observed. Similar phenomena can be found in Fig. 9d and f which show the response of S-wave velocity in the case of water and oil saturation. The only difference is the corresponding confining pressure of the transition point. It can be reasonably explained that the compliant intra-granular dissolved pores are more difficult to close than the inter-particle dissolution pores. At the relatively low confining pressure, more inter-particle dissolution pores tend to close, which leads to the P-wave velocity being greater for the # Yong 6-6. With the increasing confining pressure, especially beyond 25 MPa, some of the intra-granular dissolved pores begin to close, resulting in the enhancement of P-wave velocity for # Yong 7-2. However, as shown in Fig. 9c, the P-wave velocities of sample # Yong 6-6 are greater than sample # Yong 7-2 regardless of the increasing confining pressure. It may result from the pore fluid moderating the closure of the pore during the process of increasing confining pressure, and the main reason for the increasing P-wave velocity is the enhancement of hardness for the rock matrix and fluid. This trend for P-wave velocity is exhibited regularly as Fig. 9c and e shown. Another possible explanation could be that the squirt flow mechanism is dominant at ultrasonic frequencies when the sample mainly consists of intra-pores, which would alleviate the increase in P-wave velocities (Best et al., 1994; Best and Mccann, 1995). While for S-wave velocity in the case of fluid saturation, since the fluid shows little effect on the S-wave propagation, the dominant factor affecting the corresponding S-wave velocity is similar to that in the case of air saturation. As a result, the existence of a transition point of P- and S-wave velocities during the procedure of

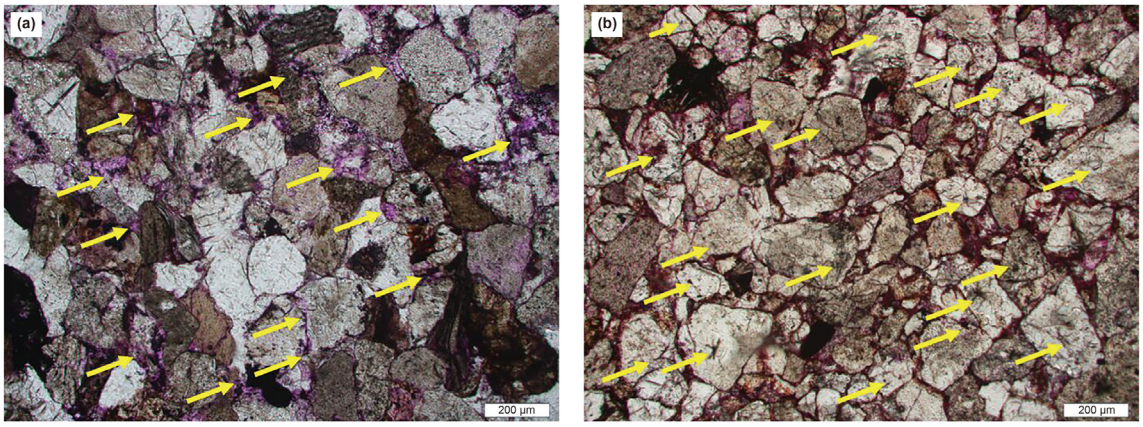

Fig. 7. Casting thin section images of samples (100X, plane-polarized light) (a) #Yong 6-6, dominant by inter-granular dissolved pores, (b) #Yong 7-2, dominant by intra-granular pores.

Table 6
Characterization of microstructure for # Yong series tight sandstone. (AS–Angularity Subround, M–Medium, GST–Grain-supported type, CAG–Contact among grains, PSLC–Primarily spot-line contact, CT–Cementation type, IDP–Inter-granular dissolved pores).

#Yong	GS, mm	V_p, m/s	V_s, m/s	Psephicity	Gradation	GST	CAG	CT	PT	Connectivity
6-6	0.25–0.50	3617	2305	AS	Fair	GS	PSLC	PC	IDP	Poor
7-2	0.25–0.50	2664	1764	AS	Fair	GS	PSLC	PC	IDP	Poor

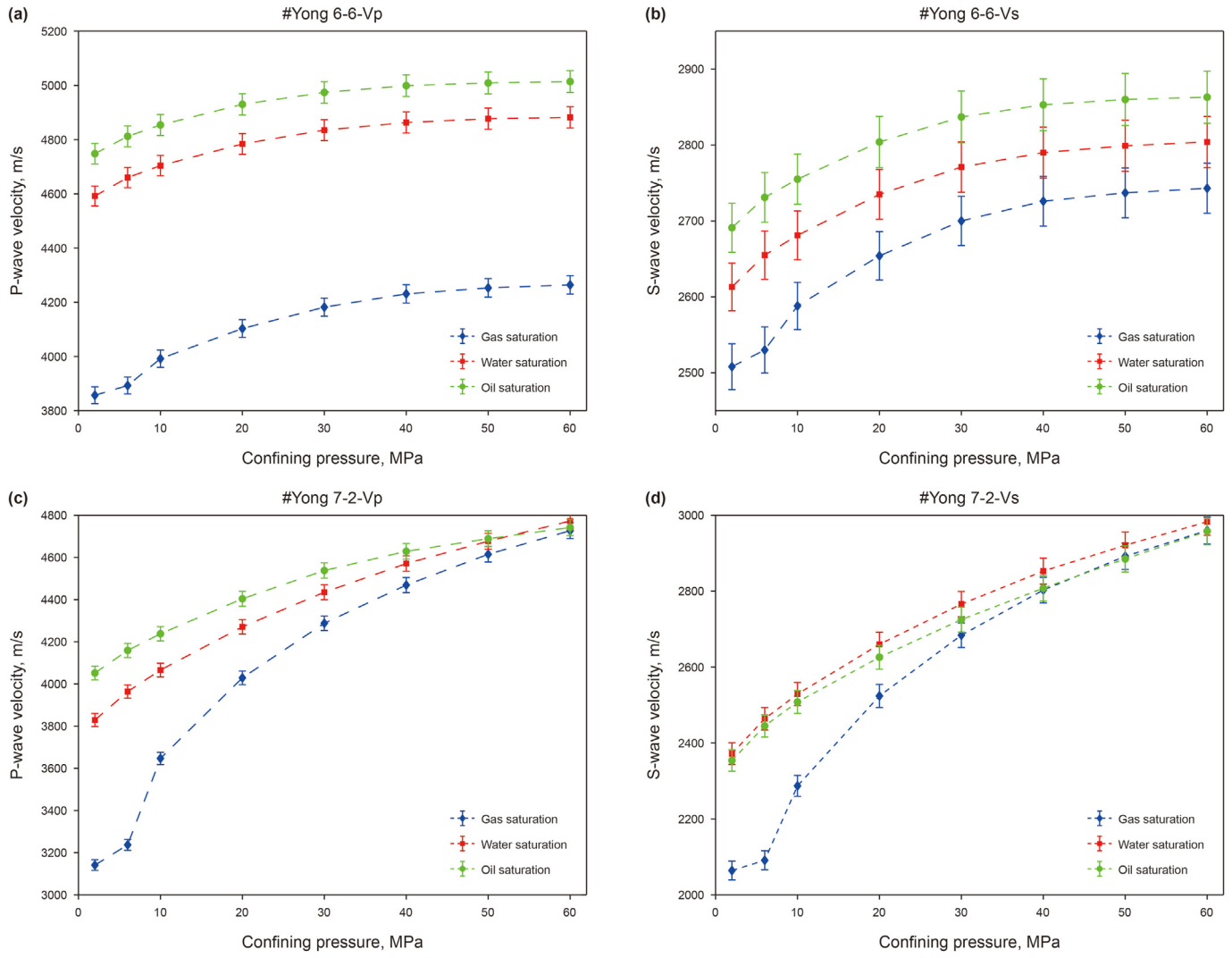

Fig. 8. Response of P- and S-wave velocities when the confining pressure is increasing under different fluids saturation. (a), (b) showed V_p and V_s in the condition of gas, water and oil saturation for sample # Yong 6-6; (c), (d) showed V_p and V_s in the condition of gas, water and oil saturation for sample # Yong 7-2.

enhancing confining pressure may also be a good indication in the dry condition to distinguish the pore type.

4.3. Grain size on the velocities

In this section, we will discuss the influence of grain size on the dynamic properties of tight sandstone. As shown in Table 3, samples # Zheng 11-2 and # Zheng 11-5 have similarities in the borehole, burial depth, porosity, density, type, and percentage of interstitial material and mineral components. Moreover, based on the casting thin section images, as shown typically in Fig. 10a and b, they also showed a similar range of pore type, septicity, gradation, grain support type, contact among grains, cementation type, and connectivity. The only difference between the two samples is the grain size. The particle size of sample # Zheng 11-2 is mainly located in the range of 0.25–0.5 mm, while for the sample # Zheng 11-5, the grain size of 0.5–1 mm is dominant. As shown in Table 7, the velocities of the samples with small grain size are greater than those of samples with large grain size at normal pressure and temperature, and the grain size seems to influence the S-wave velocity more significantly than the P-wave velocity. To further study the influence of grain size on the dynamic properties of tight sandstone, we saturated both samples with gas, brine, and oil, and investigated the response of velocities under different confining pressures. Fig. 11 shows the response of velocities for the samples with different fluid saturations. At the same confining pressure, we can always have $V_{oil} > V_{water} > V_{gas}$ for both samples. Velocities, in the case of gas saturation, are more sensitive to the increasing confining pressure. As shown in Fig. 11a, in the case of gas saturation, the P-wave velocities of both samples increase with the increasing confining pressure in the range of 0–60 MPa variation, and the velocity of a sample with a greater particle is larger than that of the small one in the range of 0–40 MPa, and reversal occurs around 40 MPa. Overall, the velocity of a sample with a large grain size is more sensitive to the variation of confining pressure with a relative growth rate of 20.7%, indicating that the large particle sample is more likely to form more compressible soft pores. Interestingly, the velocity of the small particle sample reaches its maximum at 50 MPa, while the other reaches maximum around 60 MPa, indicating that the particle contact of the small particle sample is more likely to form soft pores with a smaller aspect ratio. In the case of water saturation, the P-wave velocity of the small particle sample is generally larger than that of the greater particle sample, and the velocities of the sample with a small grain size are

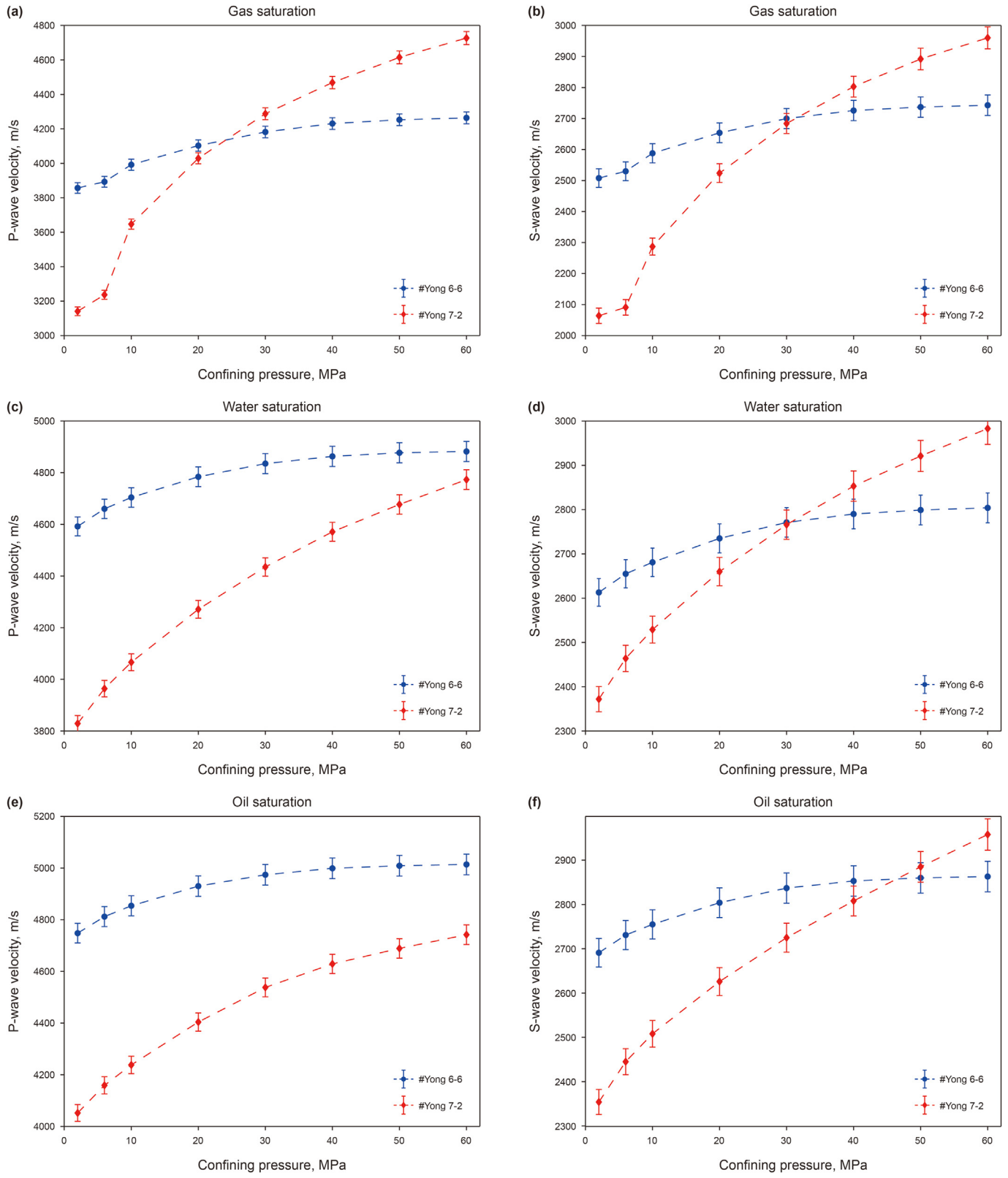

Fig. 9. Response of P- and S-wave velocities when the confining pressure is increasing under different fluids saturation. (a), (b) showed V_p and V_s in the condition of gas saturation; (c), (d) showed V_p and V_s in the condition of water saturation; (e), (f) showed V_p and V_s in the condition of oil saturation for samples # Yong 6-6 and # Yong 7-2.

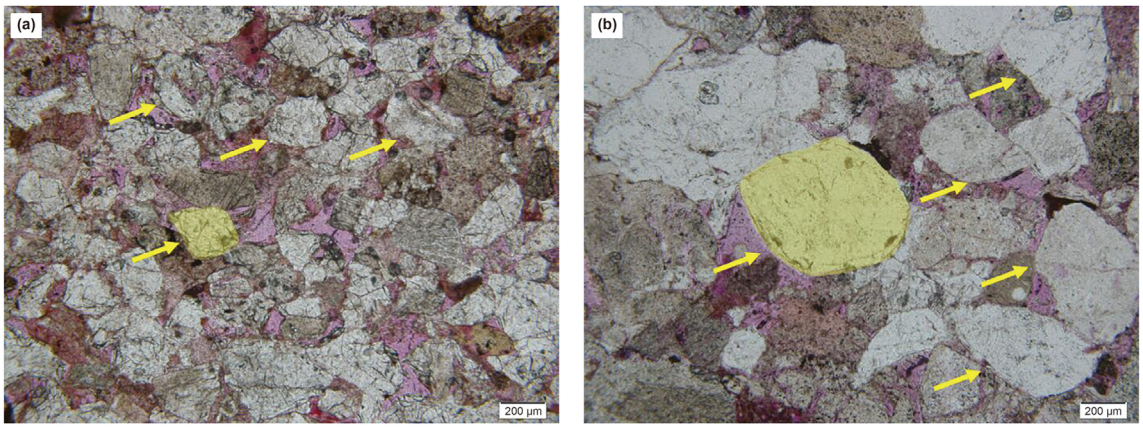

Fig. 10. Casting thin section images of samples (100X, plane-polarized light) (a) # Zheng 11-2 with range of grain size from 0.25 to 0.30 mm; (b) # Zheng 11-5 with grain size from 0.5 to 1.0 mm.

more sensitive to the confining pressure with the relative growth rate of 11.1%. With the increasing confining pressure, the differences between the velocities of two samples are gradually increased. After water saturation, some of the soft pores that are supported by water may not be easily compressed by the increasing confining pressure. The previous analysis demonstrated that the large particle samples contain more soft pores, resulting in less pressure sensitivity. In the case of oil saturation, the velocity for sample #Zheng 11-5 (great grain size) is generally larger than sample #Zheng 11-2. While the relative growth rate is similar to each other, the different response of velocity to the confining pressure at different fluid saturation may act as a specific and potential indicator to distinguish the grain size. Generally, S-wave velocities for the Zheng series samples generally show a similar variation trend to the confining pressure, and V_s of # Zheng11-2 samples are always greater than those of # Zheng11-5 samples for each case of fluid saturation.

In this study, we proposed an experimental controlling variate method by combining the usage of qualitative geological description and experimental rock physical measurements to study the response of elastic properties of tight sandstone to the varied microcosmic details of pore structure in the situation of different pore fluid (gas, brine, and oil) saturation and confining pressure. Such a method allows the clear identification of cause and effect because only one factor is different at a time so that the effect of that single factor can be determined. It is an effective toolkit to figure out the separate influence of pore structure on acoustic velocities in different conditions. Interesting phenomena can be observed to improve the precision of seismic reservoir prediction for tight sandstone reservoirs. However, due to the limitation of cored samples, only semi-quantitative relationships can be concluded. It is also rare to find a series of natural samples with the variation of only one factor, and every other is the same. In this sense, the physical modeling technique or numerical rock physical modeling should be a necessary supplement to the quantitative study of the topic.

5. Conclusions

Variations in microcosmic details of pore structure are the essential factors that influence the elastic properties of tight sandstone. With the experimental controlling variates method, we figure out the responses of velocities (V_p & V_s) to the variation of pore connectivity, pore type, and grain size separately in the conditions of different fluid saturation (gas, brine, and oil) and confining pressure. (1) In normal conditions, samples with poorer connectivity, inter-granular dissolved pores, or smaller grain size showed greater P- and S-wave velocities, or vice versa. The poorly connected sample also exhibited relatively low porosity. Additionally, the pore type was shown to have more influence on V_p than V_s, while opposite results were exhibited for the grain size. (2) P-wave and S-wave velocities of samples with varying connectedness have similar sensitivity to increasing confining pressure, with growth rates of about 17% and 15%, respectively. Samples with better connectedness at fluid saturation showed greater sensitivity to the confining pressure with a growth rate of 6.9%–11.9%, and the sensitivity is more likely controlled by connectedness than samples at gas saturation. (3) Under high confining pressure conditions, the type of fluid has no significant effect on V_p and V_s for samples with predominantly intercrystalline pores, while for samples dominated by inter-granular pores, the type of saturated fluid has a great effect on the velocity. Additionally, there exists a transition point of P- and S-wave velocities during the procedure of enhancing confining pressure in the gas saturation, which would be a good indicator to distinguish the pore type. Sample with a small grain size tends to be more sensitive to the variation of confining pressure. Observations showed that the variations of microcosmic details in pore structure have significant effects on the ultrasonic wave propagation with different fluid saturations. The relationship between the pore type and ultrasonic velocities in varied conditions can help improve the interpretation of seismic profiles and calibrate and develop rock physics models applicable to tight sandstone as well as guide the development of reservoirs.

Table 7
Characterization of microstructure for # Zheng series tight sandstone. (AS–Angularity Subround, M–Medium, GST–Grain-supported type, CAG–Contact among grains, PSLC–Primarily spot-line contact, CT–Cementation type, IDP–Inter-granular dissolved pores).

#Zheng	GS, mm	V_p, m/s	V_s, m/s	Psephicity	Gradation	GST	CAG	CT	PT	Connectivity
11-2	0.25–0.50	2329	1529	AS	M	GS	PSLC	PC	IDP	M
11-5	0.50–1.00	1887	1005	AS	M	GS	PSLC	PC	IDP	M

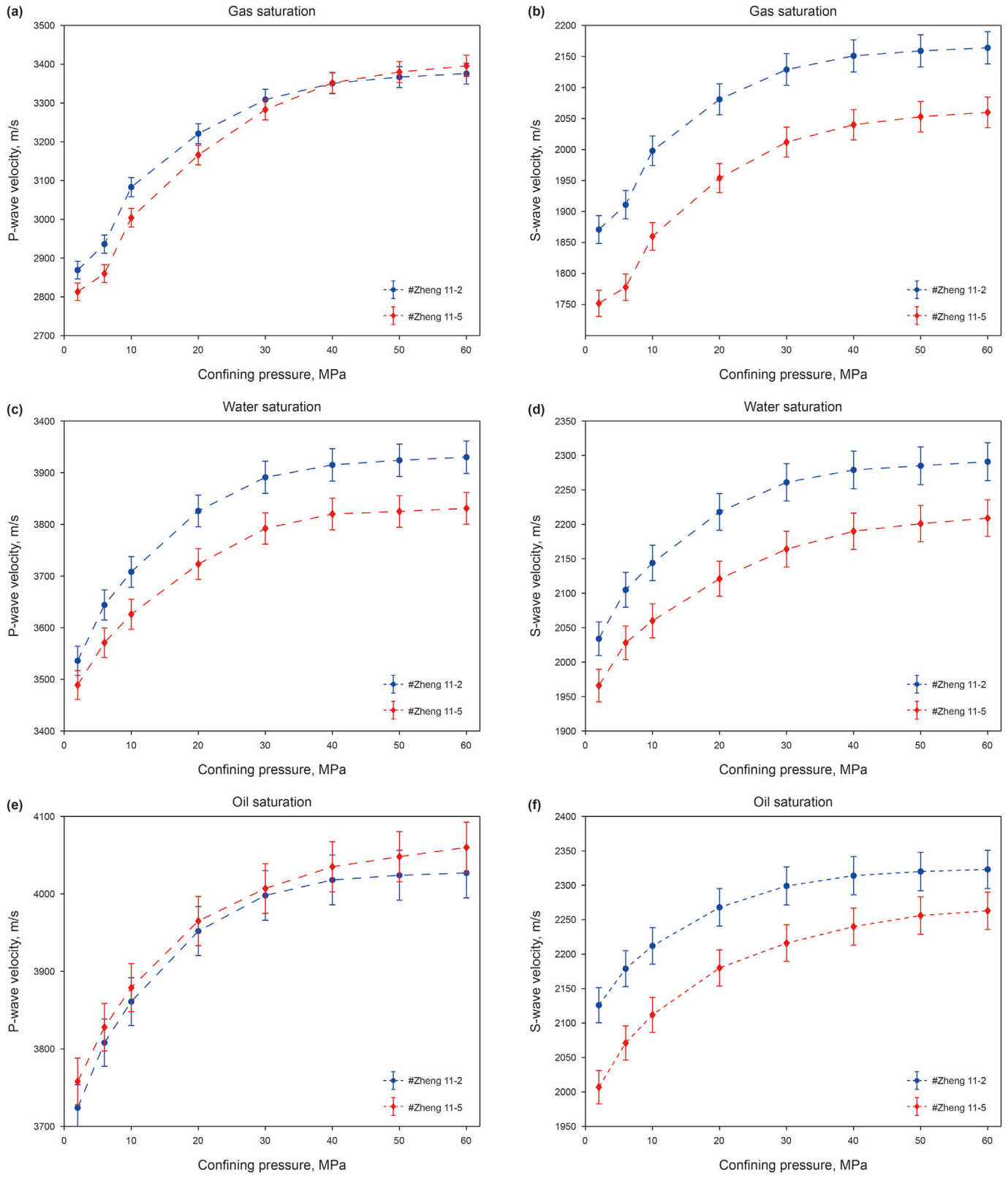

Fig. 11. Response of P- and S-wave velocities when the confining pressure is increasing under different fluids saturation. (a), (b) showed V_p and V_s in the condition of gas saturation; (c), (d) showed V_p and V_s in the condition of water saturation; (e), (f) showed V_p and V_s in the condition of oil saturation for samples # Zheng11-2 and # Zheng 11-5.

Acknowledgement

This research is supported by the Open Fund (PLC2020002, PLC20190507) of the State Key Laboratory of Oil and Gas Reservoir Geology and Exploitation (Chengdu University of Technology), National Natural Science Foundation of China (42004112, 42274175, 42030812, 41974160), and sponsored by Special projects of local science and technology development guided by the central government in Sichuan (2021ZYD0030), Natural Science Foundation of Sichuan Province (23NSFSC5311). The data or code relating to this work is available by contacting the corresponding author. There are no conflicts of interest.

References

Ambrose, R.J., Hartman, R.C., Campos, M.D., et al., 2012. Shale gas-in-place calculations Part I: new pore-scale considerations. SPE J. 17 (1), 219–229. https://doi.org/10.2118/131772-pa.

Anselmetti, F.S., Eberli, G.P., 1999. The velocity-deviation log: a tool to predict pore type and permeability trends in carbonate drill holes from sonic and porosity or density logs. AAPG (Am. Assoc. Pet. Geol.) Bull. 83 (3), 450–466. https://doi.org/10.1306/00AA9BCE-1730-11D7-8645000102C1865D.

Ba, J., Xu, W., Fu, L.Y., et al., 2017. Rock anelasticity due to patchy saturation and fabric heterogeneity: a double double-porosity model of wave propagation. J. Geophys. Res. Solid Earth 122 (3), 1949–1976. https://doi.org/10.1002/2016jb013882.

Best, A.I., Mccann, C., 1995. Seismic attenuation and pore-fluid viscosity in clay-rich reservoir sandstones. Geophysics 60 (5), 1386–1397. https://doi.org/10.1190/1.1443874.

Best, A.I., Mccann, C., Sothcott, J., 1994. The relationships between the velocities, attenuations and petrophysical properties of reservoir sedimentary rocks. Geophys. Prospect. 42 (2), 151–178. https://doi.org/10.1111/j.1365-2478.1994.tb00204.x.

Birch, F., 1960. The velocity of compressional waves in rocks to 10 kilobars: 1. J. Geophys. Res. 65 (4), 1083–1102. https://doi.org/10.1029/jz065i004p01083.

Blunt, M.J., Bijeljic, B., Dong, H., et al., 2013. Pore-scale imaging and modeling. Adv. Water Resour. 51, 197–216. https://doi.org/10.1016/j.advwatres.2012.03.003.

Cheng, W., Ba, J., Fu, L.Y., et al., 2019. Wave-velocity dispersion and rock microstructure. J. Petrol. Sci. Eng. 183 (6), 106466. https://doi.org/10.1016/j.petrol.2019.106466.

Clarkson, C.R., Freeman, M., He, L., et al., 2012. Characterization of tight gas reservoir pore structure using usans/sans and gas adsorption analysis. Fuel 95, 371–385. https://doi.org/10.1016/j.fuel.2011.12.010.

Dawson, W.C., Almon, W.R., 2002. Top seal potential of tertiary deep-water gulf of Mexico shales. Gcags Trans. 52, 167–176.

Dewhurst, D.N., Jones, R.M., Raven, M.D., 2002. Microstructural and petrophysical characterization of muderong shale: application to top seal risking. Petrol. Geosci. 8 (4), 371–383. https://doi.org/10.1144/petgeo.8.4.371.

Ding, P., Wang, D., Li, X.Y., 2020. An experimental study on scale-dependent velocity and anisotropy in fractured media based on artificial rocks with controlled fracture geometries. Rock Mech. Rock Eng. 53 (7), 3149–3159. https://doi.org/10.1007/s00603-020-02095-2.

Dong, H., Blunt, M.J., 2009. Pore-network extraction from micro-computerized-tomography images. Phys. Rev. 80 (3), 036307. https://doi.org/10.1103/physreve.80.036307.

Ebrahimi, A.N., Jamshidi, S., Iglauer, S., et al., 2013. Genetic algorithm-based pore network extraction from micro-computed tomography images. Chem. Eng. Sci. 92 (14), 157–166. https://doi.org/10.1016/j.ces.2013.01.045.

Gao, H., Li, H., 2015. Determination of movable fluid percentage and movable fluid porosity in ultra-low permeability sandstone using nuclear magnetic resonance (NMR) technique. J. Petrol. Sci. Eng. 133, 258–267. https://doi.org/10.1016/j.petrol.2015.06.017.

Ge, X., Fan, Y., Li, J., et al., 2015. Pore structure characterization and classification using multifractal theory an application in santanghu basin of western China. J. Petrol. Sci. Eng. 127, 297–304. https://doi.org/10.1016/j.petrol.2015.01.004.

Hornby, E.B., 1998. Experimental laboratory determination of the dynamic elastic properties of wet, drained shales. J. Geophys. Res. 103 (B12), 945–964. https://doi.org/10.1029/97JB02380.

Hughes, J.D., 2013. A reality check on the shale revolution. Nature 494 (7437), 307–308. https://doi.org/10.1038/494307a.

Law, B.E., Dickinson, W.W., 1985. Conceptual model for origin of abnormally pressured gas accumulations in low-permeability reservoirs. AAPG (Am. Assoc. Pet. Geol.) Bull. 69 (8), 1295–1304. https://doi.org/10.1306/AD462BD7-16F7-11D7-8645000102C1865D.

Loucks, R.G., Reed, R.M., Ruppel, S.C., et al., 2012. Spectrum of pore types and networks in mudrocks and a descriptive classification for matrix-related mudrock pores. AAPG (Am. Assoc. Pet. Geol.) Bull. 96 (6), 1071–1098. https://doi.org/10.1306/08171111061.

Ma, J., Sanchez, J.P., Wu, K., et al., 2014. A pore network model for simulating non-ideal gas flow in micro- and nano-porous materials. Fuel 116, 498–508. https://doi.org/10.1016/j.fuel.2013.08.041.

Masters, J.A., 1979. Deep basin gas trap, western Canada. AAPG (Am. Assoc. Pet. Geol.) Bull. 63 (2), 152–181. https://doi.org/10.1306/C1EA55CB-16C9-11D7-8645000102C1865D.

McCreesh, C.A., Ehrlich, R., Crabtree, S.J., 1991. Petrography and reservoir physics II: relating thin section porosity to capillary pressure, the association between pore types and throat size. AAPG (Am. Assoc. Pet. Geol.) Bull. 75 (10), 1563–1578. https://doi.org/10.1306/0C9B2993-1710-11D7-8645000102C1865D.

Mousavi, M., Bryant, S., 2007. Geometric models of porosity reduction mechanisms in tight gas sands. In: Rocky Mountain Oil and Gas Technology Symposium. April 16-18, Denver Colorado. https://doi.org/10.2118/107963-MS.

Nelson, P.H., 2009. Pore-throat sizes in sandstones, tight sandstones, and shales. AAPG (Am. Assoc. Pet. Geol.) Bull. 93 (3), 329–340. https://doi.org/10.1306/10240808059.

Oukhlef, A., Champmartin, S., Ambari, A., 2014. Yield stress fluids method to determine the pore size distribution of a porous medium. J. Non-Newtonian Fluid Mech. 204, 87–93. https://doi.org/10.1016/j.jnnfm.2013.12.004.

Passey, Q.R., Bohacs, K., Esch, W.L., et al., 2010. From oil-prone source rock to gas-producing shale reservoir-geologic and petrophysical characterization of unconventional shale gas reservoirs. In: International Oil and Gas Conference and Exhibition in China. Society of Petroleum Engineers. https://doi.org/10.2118/131350-MS. SPE-131350-MS.

Peng, S., Marone, F., Dultz, S., 2014. Resolution effect in X-ray microcomputed tomography imaging and small pores contribution to permeability for a berea sandstone. J. Hydrol. 510, 403–411. https://doi.org/10.1016/j.jhydrol.2013.12.028.

Ruiz, F., Cheng, A., 2010. A rock physics model for tight gas sand. Lead. Edge 29 (12), 1484–1489. https://doi.org/10.1190/1.3525364.

Sakhaee-Pour, A., L, B.S., 2014. Effect of pore structure on the producibility of tight-gas sandstones. AAPG (Am. Assoc. Pet. Geol.) Bull. 98 (4), 663–694. https://doi.org/10.1306/08011312078.

Si, W., Di, B., Wei, J., et al., 2016. Experimental study of water saturation effect on acoustic velocity of sandstones. J. Nat. Gas Sci. Eng. 33, 37–43. https://doi.org/10.1016/j.jngse.2016.05.002.

Smith, T.M., Sayers, C.M., Sondergeld, C.H., 2009. Rock properties in low-porosity/low- permeability sandstones. Lead. Edge 28, 48–59. https://doi.org/10.1190/1.3064146.

Spencer, C.W., 1989. Review of characteristics of low-permeability gas reservoirs in western United States. AAPG (Am. Assoc. Pet. Geol.) Bull. 73 (5), 613–629. https://doi.org/10.1306/44B4A23A-170A-11D7-8645000102C1865D.

Surdam, R.C., 1997. A new paradigm for gas exploration in anomalously pressured" tight gas sands" in Rocky Mountain Laramide basins. Mem. Am. Assoc. Petrol. Geol. 67, 283–298. https://doi.org/10.1306/M67611C17.

Verwer, K., Eberli, G., Baechle, G., et al., 2010. Effect of carbonate pore structure on dynamic shear moduli. Geophysics 75, E1–E8. https://doi.org/10.1190/1.3280225.

Verwer, K., Eberli, G.P., Weger, R.J., 2011. Effect of pore structure on electrical resistivity in carbonates. AAPG (Am. Assoc. Pet. Geol.) Bull. 95 (2), 175–190. https://doi.org/10.1306/06301010047.

Weger, R.J., Eberli, G.P., Baechle, G.T., et al., 2009. Quantification of pore structure and its effect on sonic velocity and permeability in carbonates. AAPG (Am. Assoc. Pet. Geol.) Bull. 10 (93), 1297–1317. https://doi.org/10.1306/05270909001.

Xie, J., Cao, J., Schmitt, D.R., et al., 2019. Effects of kerogen content on elastic properties-based on artificial organic-rich shale (AORS). J. Geophys. Res. Solid Earth 124 (12), 12660–12678. https://doi.org/10.1029/2019jb017595.

Xu, L., Liu, X., Liang, L., 2014. A pore network model reconstruction method via genetic algorithm. J. Nat. Gas Sci. Eng. 21, 907–914. https://doi.org/10.1016/j.jngse.2014.09.038.

Yan, F., Han, D., 2015. Effect of pore geometry on gassmann fluid substitution. Geophys. Prospect. 64 (6), 1575–1587. https://doi.org/10.1111/1365-2478.12348.

Yang, Y.S., Liu, K.Y., Mayo, S., et al., 2013. A data- constrained modelling approach to sandstone microstructure characterisation. J. Petrol. Sci. Eng. 105 (3), 76–83. https://doi.org/10.1016/j.petrol.2013.03.016.

Yin, H., 1992. Acoustic Velocity and Attenuation of Rocks: Isotropy, Intrinsic Anisotropy, and Stress Induced Anisotropy. Ph.D. thesis. Stanford University.

Zhang, L., Ba, J., Carcione, J.M., 2021. Wave propagation in infinituple-porosity media. J. Geophys. Res. Solid Earth 126 (4), e2020JB021266. https://doi.org/10.1029/2020JB021266.